N94- 30444

SENSING THE GAS METAL ARC WELDING PROCESS

N. M. Carlson, J. A. Johnson, H. B. Smartt, A. D. Watkins, E. D. Larsen, P. L. Taylor, and M. A. Waddoups

Idaho National Engineering Laboratory
P.O. Box 1625, Idaho Falls, ID 83415-2209

ABSTRACT

Control of gas metal arc welding (GMAW) requires real-time sensing of the process. Three sensing techniques for GMAW are being developed at the Idaho National Engineering Laboratory (INEL). These are (1) noncontacting ultrasonic sensing using a laser/EMAT (electromagnetic acoustic transducer) to detect defects in the solidified weld on a pass-by-pass basis, (2) integrated optical sensing using a CCD camera and a laser stripe to obtain cooling rate and weld bead geometry information, and (3) monitoring fluctuations in digitized welding voltage data to detect the mode of metal droplet transfer and assure that the desired mass input is achieved.

NONCONTACTING ULTRASONIC SENSOR SYSTEM

The ultrasonic sensor detects defects in the solidified weld metal on a pass-by-pass basis [1,2,3,4] for a multipass, pulsed GMAW process on thick section (31.8 to 41.3 mm, 1.25 to 1.625 in.) welds. The sensor is being developed under the Programmable Automated Welding System (PAWS) project. The noncontacting sensor system [5] has two sensor components, an ultrasound generating source and an ultrasound detector, as well as a remotely located computer data acquisition and processing unit.

The ultrasound is generated by a short duration, 11 ns, light pulse from an Nd:YAG laser with an exit beam power of 56 mJ/pulse. The 1 mm laser spot is delivered at a 20 Hz rate to the solidified top surface of the weld several inches behind the electrode using focusing optics mounted on the laser head [6,7]. The ultrasonic detector is an EMAT and amplifier designed and fabricated for PAWS at the National Institute of Standards and Technology in Boulder, Colorado [8]. The permanent magnet EMAT induces a magnetic field in the weld sample. The sound generated by the laser pulse interacts with the magnetic field, changing an associated electrical field. This interaction is detected by a pickup coil. The signal is then evaluated as an ultrasonic A scan. The ultrasonic system includes the hardware and software necessary to monitor the condition of the solidified weld metal while receiving and sending information to the weld controller about the quality of the solidified weld bead.

Pulsed Laser Sound Generation

A first step in devising a noncontacting technique for sensing defect generation in the welding process is to develop a method for generating sound waves in the material. In this system, ultrasound is generated by a focused, 1 mm (0.039 in.) diameter laser spot from a pulsed Nd:YAG laser operating at 1064 nm. The short duration, 11 ns, laser pulse has a peak intensity of 10^7 W/cm^2 and generates high frequency, broadband ultrasound in the solidified weld metal by surface ablation. The sound waves arrive at the top surface of the weld sample, where they are received by the EMAT, after reflecting or mode converting at the bottom surface of the sample.

For the PAWS demonstration, the compact laser head is mounted on a weld head. The laser head is 533 x 178 x 127 mm (21 x 7 x 5 in.) and 7.7 kg (17 lbs). The rugged laser head design provides optics sealed from the environment. To assure safe operation of the laser, the shutter and the high voltage supply are disabled by either computer or manual control. The laser head is connected to the laser power supply by an umbilical that supplies power and cooling to the laser head. A focusing optics fixture that houses a 50-50 beamsplitter, optional neutral density filters, and a 300 mm (11.8 in.) focusing lens is mounted in front of the laser to form the 1 mm (0.039 in.) spot size on the solidified weld bead.

EMAT Receiver

The basic components of an EMAT are a magnet, a conducting pickup coil, and amplifying electronics. The EMAT sensor assembly is 105 x 68.6 x 157 mm (4.13 x 2.70 x 6.18 in.). The height includes the cable to the associated electronics. The overall length increases to 163.5 mm (6.44 in.) with the addition of wheels to facilitate the movement of the EMAT down the weld sample. In Figure 1 the laser and EMAT are shown mounted to the carriage of a sidebeam welder. In the demonstration system, the components will be mounted on the weld head of a crawler; the detection approach is the same for both fixturings of the sensor components.

The EMAT produces a magnetic field in the sample using a neodymium-iron-boron permanent magnet. A magnetic pole-piece is placed between the permanent magnet and the pickup coil to intensify the magnetic field at the EMAT coil. The arriving laser-generated sound field causes the charges in the metal to move in the magnetic field, which generates a secondary field that is detected by a small pickup coil. The conducting pickup coil is a 25-turn counter wound, center tapped, coil mounted behind a stainless steel plate. The entire unit is designed to be sensitive to incident shear waves arriving at 45° with a frequency range of 0.5 to 2.0 MHz. The EMAT is sensitive to a minimum flaw size of 1 mm (0.039 in.) in the plane of the ultrasonic wave perpendicular to the direction of weld travel.

Effective operation of the EMAT also requires amplification of the received signal; this is accomplished by a preamplifier and a narrowband amplifier. The high gain, low noise preamplifier consists of two electronic circuit boards, located in the EMAT assembly, that provide common mode rejection and signal amplification of approximately 60 dB. The narrowband amplifier is located near the sensor computer away from the EMAT assembly and welder. This amplifier rejects electromagnetic interference picked up by the EMAT assembly and the 6.7 m (22 ft) signal cable, amplifies the signal by 20 dB, filters noise outside the signal bandpass, and outputs a signal to a 50 ohm load.

For the EMAT assembly to operate effectively on a weld sample, the pickup coil needs to be ~0.16 mm (6 mil) or less above the sample. To achieve this standoff distance and to allow the EMAT to move easily over the part being inspected, the EMAT is equipped with wheels. The wheels are electrically isolated from the weld sample using nonconducting shaft sleeves to avoid electrical interference from the welder. The EMAT assembly is attached to the welding head by a mounting fixture; the weight of the EMAT is supported by weld sample. The path that the laser and the EMAT follow is dictated by the path of the crawler weld head; the sensor components are positioned at the start of the welding pass and not relocated during the pass. Thus, for the demonstration system, the sensor is used on linear welds with the EMAT and laser moving parallel to the weld centerline. With the addition of servo motors, it would be possible for the EMAT and laser to inspect nonlinear weld parts.

Figure 1. Ultrasonic sensor components mounted on sidebeam welder.

Because the EMAT assembly is close to the preheated weld sample, external cooling is required to keep the magnet well below its Curie temperature and to cool the electronics enclosed in the EMAT assembly. The EMAT is currently designed to be placed on a plate preheated up to 93°C (200°F). Dry nitrogen or argon at -4°C and 6.9 x 10^4 Pa (25°F and 10 psi) is used as

the cooling medium. The cooling line is attached to a 6.35 mm (0.25 in.) electrically isolated line tube located on the top of the EMAT assembly.

Computer System

The computer system for the ultrasonic sensor acquires and processes information from the EMAT and determines if the weld is of acceptable quality. Information about unacceptable weld is sent to the weld controller. The central processing unit of the ultrasonic sensor is a full-featured 80486 based PC/AT compatible with a clock speed of 25 MHz. The CPU board has 4 megabytes of RAM memory, on chip memory cache, math co-processor, small computer systems interface and floppy controllers, and keyboard and VGA monitor ports. When the system is powered up, the watch-dog timer assures the successful start or restart of the system. The keyboard and monitor are necessary during the system integration and debugging phases. For the demonstration, the system operates without the keyboard or monitor.

A read-only solid state disk emulator and a read/write daughter board are used for storage of the operating system and data acquisition and processing software, and for temporary file storage of calibration and initialization values. The solid state disk emulator is equipped with an onboard PROM programmer. Utility software is available to copy files and programs onto the solid state disk emulator via a floppy disk.

A watch-dog timer/communication port card is used to reboot the sensor when the system crashes or hangs up due to an unexpected event. The watch-dog timer is equipped with a variable timer that is set by the sensor software. Before the end of each period the sensor software sets a bit in the register of the card. However, if the bit is not set before the end of the set period, the card provides a low-going TTL signal that is used to reset the CPU using auto restart routines. A card is also provided on the receiver and transmit lines to protect the computer from high-level common mode voltage spikes.

An RS-422 interface is used to communicate with the weld controller. If unacceptable weld is detected, the ultrasonic sensor system computer streams data packets about this condition to the controller via the RS-422 interface. Throughout the welding operation, data packets are communicated over the interface between the sensor and the controller.

A waveform analyzer board analyzes the incoming EMAT signals. The board is externally triggered by a synchronization pulse from the laser. The board, operating in the peak detection mode, detects the presence of signals in two calculated time windows. The presence or absence of the signals in the selected time windows indicates the quality of the weld and the health of the sensor system, as explained below.

The laser exit beam is controlled by the computer to ensure that the beam is only present when required for calibration and data acquisition. The signals to open the shutter and enable the high voltage creating the exit beam are sent to the laser from the digital I/O board. The status of the enable and disable of the beam on the digital I/O board is under the control of the ultrasonic sensor system's CPU. The CPU card, back plane, and necessary boards are housed in an industrial chassis in an environmental rack.

Defect Detection Approach

Ultrasound data are acquired and processed by the ultrasonic sensor system to determine the quality of the weld pass. The presence of good quality weld results in two signals being detected by the system. One signal, referred to as the detection signal, indicates the quality of the weld. The second signal, referred to as the health signal, indicates the operational quality of the ultrasonic sensor system. In the presence of a defect condition, such as incomplete penetration or porosity, the sound path of the detection signal is disrupted, resulting in a decrease in signal amplitude or complete loss of the signal. A confidence level evaluation is made by monitoring the amplitude of the health signal in a time window that is not likely to be altered by unacceptable weld quality. The health signal provides a means of determining that loss of the detection signal is due to a defect condition rather than to an equipment problem.

In the detection approach used for the ultrasonic sensor, there are three preparatory steps before acquiring data during a weld pass. The system completes acknowledgment and calibration sequences. Data describing the next weld pass geometry are then down loaded from the off-line programmer. These data are used by the ray tracing program in the initialization sequence to calculate the position of the laser and EMAT needed to direct sound through the critical fusion zone. Ray tracing also provides the arrival time and tangential displacement values of the signals of interest for monitoring the weld pass. These times are used by the computer to set the time gates on the waveform analyzer. The displacement values are used to determine the expected wave amplitude of arriving signals when no defects are present in the weld.

The sensor system can store the voltage of the detection signal for system debugging. This information can be plotted against distance along the weld centerline. Distance information is approximated using the expected travel speed; therefore, distance values can vary by up to 12.7 mm (0.5 in.). Figure 2 shows such a plot for the fourth weld pass on a 31.8 mm (1.25 in.) V-groove weld sample. The area of interest for detecting defects is the sidewall between passes three and four.

Based on the results of the calibration and initialization sequences, the threshold for acceptable weld is placed at 1.2 V. Therefore, all voltage values above 1.2 indicate acceptable weld. The system threshold can be adjusted to increase or decrease sensitivity depending on the requirements of the welding application. Three consecutive signals above or below threshold are required for the sensor to call an area acceptable or unacceptable; this avoids defect calls resulting from minor surface variations or transient fluctuations in the laser power.

The sample was radiographed to confirm the location of incomplete sidewall penetration for sensor system validation. From the radiograph, areas of continuous incomplete penetration are located between 178 and

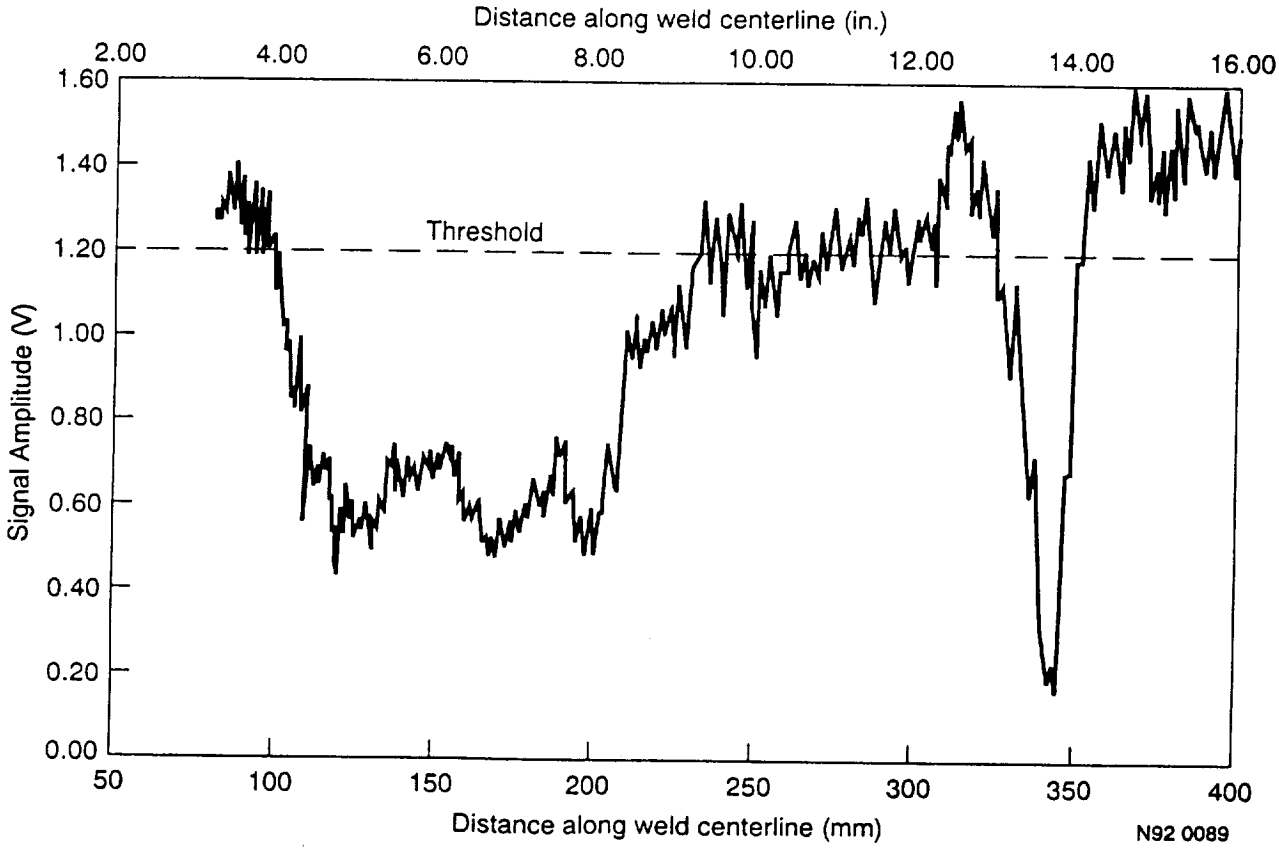

Figure 2. Distance vs. voltage for fourth weld pass.

279 mm (7.0-11.0 in.) and at 318 mm (12.5 in.). The ultrasonic system identified incomplete penetration in these areas as signal voltages are below the 1.2 V threshold (see Fig. 2). The sensor system detected other areas of intermittent incomplete penetration that were confirmed by the radiograph. Mild incomplete penetration is present in the first 381 mm (15 in.) of weld. The only area of good weld is from 381 mm (15 in.) to the end of the distance monitored. The sensor system's ability to detect incomplete penetration was validated for other selected passes using the procedures described above. Those tests confirmed the system's ability to detect incomplete penetration under GMAW conditions with travel speeds varying from 178 to 227 mm/min (7-9 in./min).

Ultrasonic Sensor Summary

An ultrasonic sensor system can be used to detect defects on a pass-by-pass basis when joining thick section plate using pulsed GMAW. The system is noncontacting and presents no weld contamination problems. The present system can detect defects in linear sections of weld on plate preheated to 93°C (200°F); a pulsed laser is used to generate ultrasound and an EMAT to receive the ultrasound. A PC-based computer system controls data acquisition and processing. When a defect condition is detected, the sensor computer alerts the controller that weld of unacceptable quality is being made. The sensor system provides the controller with defect information at 4 Hz for feed-back control of the GMAW process.

INTEGRATED OPTICAL SENSOR

An automated welding system must be capable of adapting to changing conditions encountered during the welding process. Many sensor systems have been developed to give automated welding systems the capability to adapt to variations in one parameter, e.g., laser striping for joint tracking [9], through-the-arc sensing [10], coaxial viewing of the weld pool [11], and infrared sensing [12]. The integrated optical sensor (IOS) is a multifunction, feedback control sensor that performs three distinct near-real-time measurements: weld pool position and width, standoff, and weld bead centerline cooling rate. The pool position and width are used to control the welding torch position relative to the weld pool, allowing the weld controller to compensate for such phenomena as arc blow. The welding system uses the sensor standoff distance in a feedback loop to control the contact-tip-to-work-piece distance. Cooling rate information is used to infer the final metallurgical state of the weld bead and heat-affected zone; therefore, postweld mechanical properties can be controlled.

The IOS consists of three major components: a remote head CCD camera with lens and filter pack, a continuous wave Ga-Ar diode laser, and a remotely located computer data acquisition and processing unit. The sensor head is mounted just behind the welding torch as pictured in Figure 3. The sensor's camera and laser are mounted in an industrially hardened case, allowing the sensor head to withstand harsh operating environments without any specialized cooling or power requirements. A cable attaches the sensor head to the computer data acquisition system. The computer processing system acquires images from the sensor's camera and analyzes them for weld pool width/position, standoff, and weld bead centerline cooling rate. Data are transmitted to the weld controller via an RS-422 serial interface at a rate up to 10 Hz.

Sensor Operation

The IOS is a stand-alone system that operates with minimal operator assistance. When the power is turned on the sensor computer is activated and boots the operating system, which then automatically starts the sensor software. The camera and laser power are activated and readied for operation. Once this has taken place, the sensor waits for an input command from the RS-422 serial communication port.

A calibration block centered underneath the IOS is used to calibrate the image intensity and distance measurements. The calibration procedure ensures that the level of illumination received by the camera is appropriate so that the temperature measurements made for the cooling rate calculation will be correct. The standoff is used to ensure that the correct distance values are reported. As long as the sensor-to-torch relationship is constant, the calibration need not be re-performed. When the calibration process ends, the sensor sends the calibration

complete command to the controller and is ready to acquire data.

During data acquisition, images are obtained with the frame grabber in the processing computer; the output data are determined and sent to the controller at a rate of up to 10 Hz. During sensor operation, the controller uses various commands to control the sensor. For example, the sensor may be paused and then continued. While the sensor is paused the laser shutter is closed and the sensor stops collecting data. The data output rate can be varied from 1 to 10 Hz by the controller. The temperature set point (the point at which the weld bead cooling rate is determined) may be changed, as well as the weld travel speed.

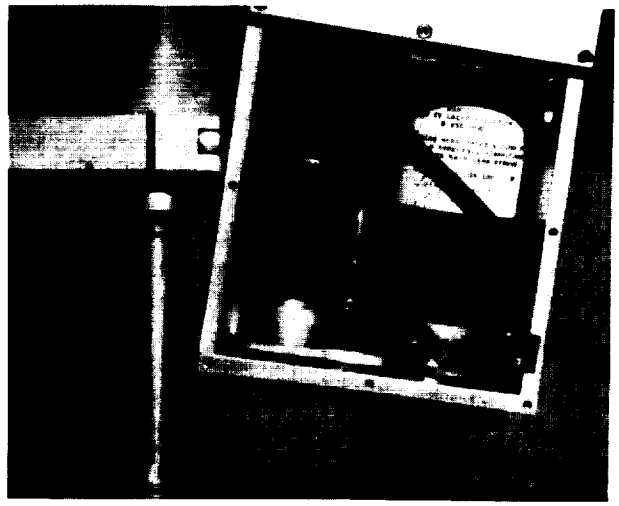

Figure 3. Sensor head with cover plate removed; remote CCD camera head is on left and diode laser on right.

Sensor Hardware

The sensor head, which is approximately 117 mm wide, 127 mm high, and 73 mm thick (4.6 x 5 x 2.9 in.) carries the camera and laser behind the welding torch. The sensor head is mounted on the welding torch at a slight angle so that the edge of the welding torch gas cup is visible in the image. This viewing angle ensures that the camera does not receive too much light from the welding arc. The camera view is approximately 63 x 45 mm (2.5 x 1.8 in.) at a standoff of 140 mm (5.5 in.). The diode laser supplies an infrared beam that is spread into a line using a cylindrical lens located in the lower portion of the laser housing. At the bottom of the laser housing is a shutter mechanism for controlling the laser beam. Underneath the laser are two mirrors that reflect the beam out of the IOS housing at the proper angle. All power, controls, and video signals are carried in a single umbilical cord from the sensor computer and laser control system. A diagram of the system is shown in Figure 4.

The IOS uses an industrial PC/AT compatible 80486 with 8 MB of memory, operating at 25 MHz, for data processing. The computer system is designed for stand-alone operation and does not require the use of a monitor or keyboard. The computer sends and receives data via an RS-422 serial communication port connected to the controller. A frame grabber is used to translate video images into arrays of pixel data. An analog and digital output board is used for interfacing with the laser shutter and camera gain controller. A watch-dog timer and a temperature monitor board are also installed in the computer. The watch-dog timer reboots the system if the computer "locks up" and is no longer processing data. The temperature monitor measures the internal temperature of the computer's case and can be used to send warning to the operator in the event of overheating. An electronic disk stores the software, thus avoiding the use of a more delicate hard disk. A floppy disk is required only for loading the software onto the electronic disk.

Sensor Software

The sensor software makes all the calculations for data output, as well as controlling the camera gain and laser shutter. To obtain the desired data output rate, the software was written using a 32 bit C compiler, which produces code that, with the help of a DOS extender, allows the software to take advantage of the protected mode of the 80486 CPU [13]. Protected mode allows the software to access all the memory installed in the machine and run approximately twice as fast as the same software would run in the typical real mode used by DOS [14].

To calculate output data, the computer obtains images of the weld pool from the camera and converts them into an array of numbers ranging from zero to 256 using a frame grabber residing on the I/O bus. The array of image data is available to the computer as part of the computer's protected memory. The array of pixels in

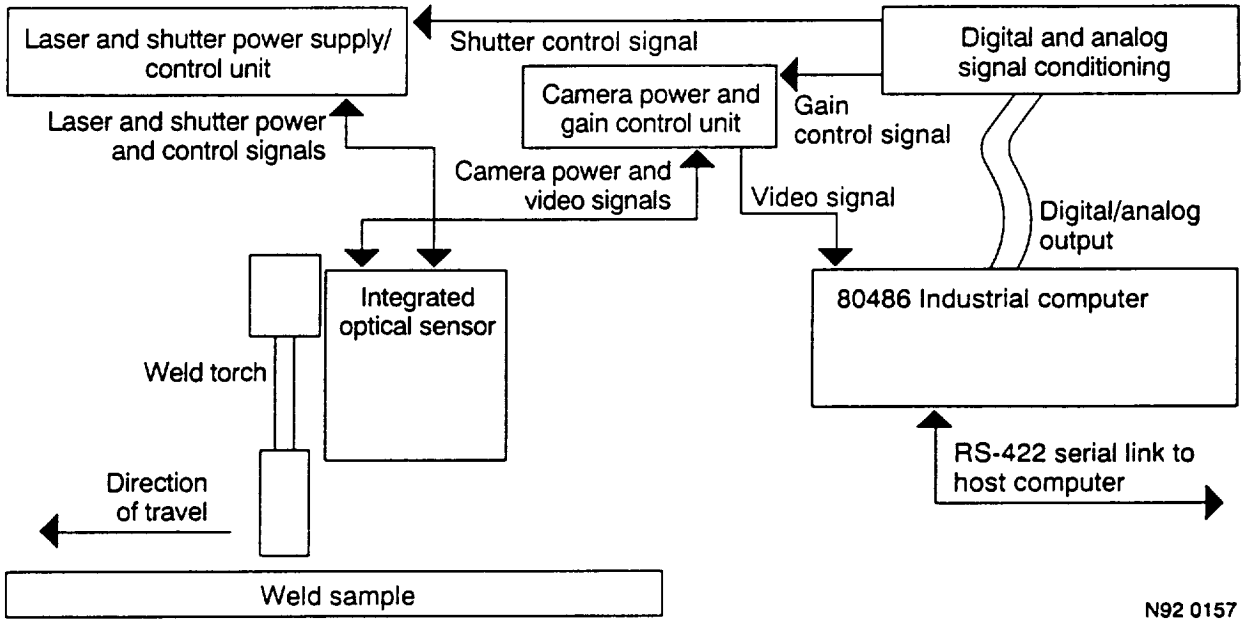

Figure 4. Diagram of IOS sensor system components.

memory is analyzed for intensities and object locations using common image processing techniques [15,16].

Data processing operations locate the edges of the molten weld pool, calculate the center of the weld pool, and scan the image at the center location. The laser line data and data from the calibration sequence are used to determine the standoff for each edge of the weld bead in millimeters. Cooling rate is determined using the scan of the image along the weld centerline. An exponential or linear equation is fit to the scanned data. The slope of the curve is then calculated, and with the travel speed data, converted into a cooling rate in Centigrade degrees per second. When all calculations are complete the data are sent to the controller. The complete processing time for all data operations is approximately one tenth of one second.

Sensor Calibration

The measurement of the step on the calibration block is used to develop a scale factor normal to the weld centerline; the scale factor along the weld centerline is derived using the known aspect ratio of the frame grabber. The known height of the step on the calibration block is used to determine a standoff scaling factor. With the known standoff sent from the controller, the sensor can determine the zero point for referencing laser line movement. The scale factors and the reference point are then used to calculate real-world measurements before they are sent to the controller.

The temperature measurement function of the sensor is used to determine cooling rate. The sensor uses the camera to detect the infrared radiant energy from the surface of the weld metal. The level of radiant energy indicates the temperature. For the measurements to be consistent, the camera gain setting is adjusted during the calibration procedure. The computer simply evaluates the level of brightness of the image received during the calibration procedure and adjusts it, using the camera gain control, to a predetermined level.

For the infrared energy received by the camera to reflect the real temperature of the material, the camera is evaluated using a black body source. ("A black body, or ideal radiator, is a body which emits and absorbs at any temperature the maximum possible amount of radiation at any given wavelength." [17]) The camera is aimed at the black body source and the pixel levels are recorded for temperatures set throughout the range of the source. The IOS reads temperatures in the range of 982 to 1425 C° (1800 to 2600 F°).

Integrated Optical Sensor Summary

The IOS is a multifunction feedback control sensor that makes three distinct measurements in near real time: weld pool position and width, standoff, and weld bead centerline cooling rate. Weld pool position and width are used by the weld controller to control the position of the weld pool in relation to the joint. The standoff is used to control contact-tip-to-work-piece distance based upon the distances measured from the sensor to each edge of the weld bead. Cooling rate information is used to infer the final metallurgical state of the weld bead and heat-affected zone.

Because of the sensor's small size, it mounts unobtrusively behind the welding torch; previous infrared measurement devices were too large to mount behind the welding torch. Since the IOS uses standard off-the-lab-shelf components, the cost of the sensor is relatively low, enabling the technology to be more readily utilized.

DYNAMICS OF DROPLET DETACHMENT

Growth and detachment of droplets in GMAW play an important role in predicting the heat and mass transfer to the weld pool. Previous work [18,19] shows that the droplets not only have momentum but also carry approximately 47% of the total heat transferred to the weld pool. Droplet size and detachment frequencies are important in controlling weld pool shape and solidified weld microstructure.

GMAW exhibits various modes of droplet transfer. With 98% argon/2% oxygen shielding gas, the common modes of transfer are globular, spray, streaming spray, and rotating spray transfers. Lesnewich [20] showed that the mode of metal transfer depends on process variables such as welding current, electrode extension, electrode diameter, and polarity. He showed that there is a sharp transition between the globular and spray modes of metal transfer that occurs at specific process variables. In the transition from the globular to spray transfer modes, the droplet detachment frequency dramatically increases while the droplet size correspondingly decreases. Recently, however, other researchers [19,21] have found that the globular to spray transition occurs over wider ranges of variables. Clark [19] suggested that during the transition from globular to spray, droplet size and detachment frequency bifurcate between larger droplet sizes and longer detachment times (globular) and smaller droplet sizes and shorter detachment times (spray) as electrode speed is increased.

Modeling and control of GMAW require both theoretical and experimental investigations into the physics of the process [20,22,23]. Several theories, such as force balance [24,25] and pinch instability [26,27], have been proposed to explain the droplet transfer. Limited success was obtained in predicting transfer mode. The models do not account for bifurcations in droplet detachment frequencies and size during the transition between globular and spray transfer modes. Measuring the dynamics of the metal transfer mode in GMAW is part of an ongoing effort. In the globular transfer region such measurements are mainly of academic interest and provide grist for the theoreticians and modelers. In the spray region these measurements may lead to new insights into the process, resulting in methods of controlling droplet transfer, and thus potentially controlling droplet momentum, which may have important implications for controlling the depth of penetration and other parameters of the weld pool.

Experimental Investigation

Data are acquired over a wide range of electrode speeds to analyze the transition of metal transfer from globular to spray. In previous work, [28,29] analysis of high-speed film data taken synchronously with the electrical data has been presented. Those preliminary results indicated a possible transition from a single frequency and droplet size to a bifurcation and then to a chaotic transfer. This section reports on measurements of the voltage and current over a range of electrode speeds encompassing the transition region in an attempt to confirm this transition to chaotic transfer [30].

Welding Parameters

The electrode speed was changed to obtain the variation in transfer mode, with the contact-tip-to-workpiece distance, the open-circuit voltage, the materials and the travel speed kept constant for most of the measurements (see Table 1). At very low electrode speeds, the travel speed had to be decreased to obtain a stable arc.

Electronic Data Acquisition System

The system is similar to that described in [28]. The major change was to provide the capability to use significantly longer data acquisition periods. The sampling rate was decreased from 50 to 10 kHz and transient digitizers with 128k, instead of 8k, of memory were used. These changes made acquisition times of up to 13.1 s, in contrast to 0.164 s, possible. Thus a significantly larger number of droplet transfer events can now be observed. A schematic of the system is shown in Figure 5. Other changes included a more accurate calibration of the system and improved amplification and filtering. Both the current and voltage data had an analog 3 dB bandwidth between 0.3 and 3000 Hz. Some of the data were subsequently digitally filtered to a narrower bandwidth as required for different analyses. The system was calibrated by acquiring signals from a source with known sinusoidal voltage at several frequencies in the bandwidth.

Table 1. Welding Parameters

Electrode Speed	55 - 170 mm/s	Power-Supply Slope	0.004 V/A
Travel Speed	1.0 - 4.2 mm/s	Electrode Diameter	0.889 mm
Contact-Tip-to-Workpiece Distance	15.9 mm	Electrode Composition	AWS A5.18, ER70S-3
Open-Circuit Voltage	27.0 V	Shield-gas Flow	14.2 L/min
Shielding Gas	Ar - 2% O		

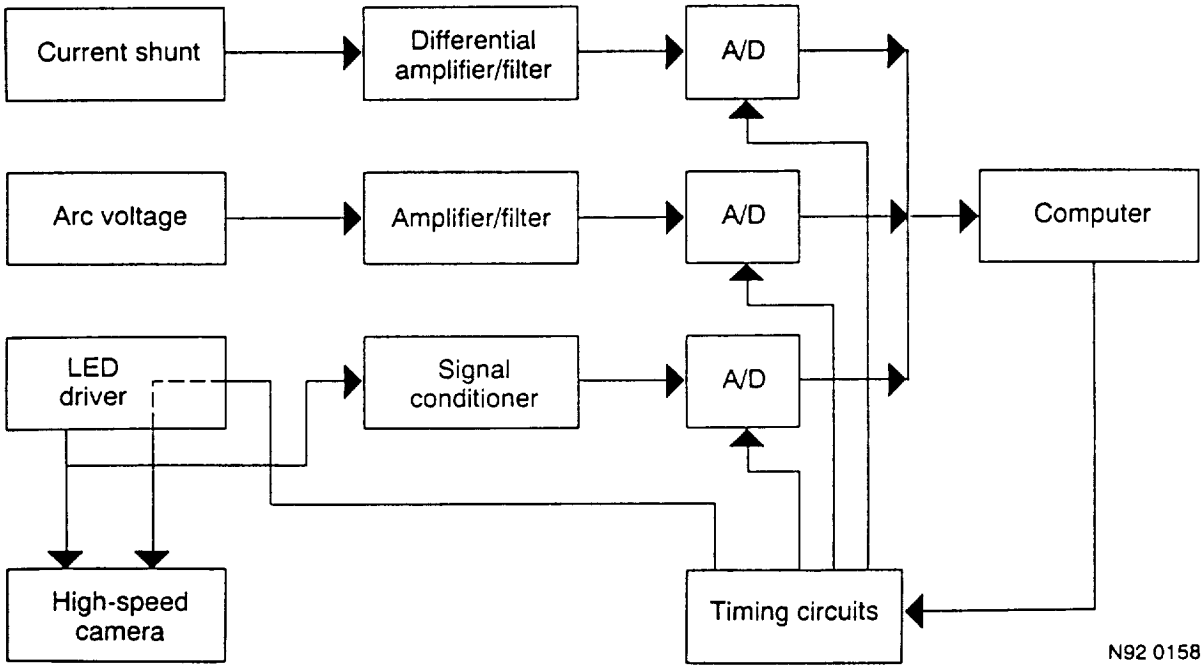

Figure 5. Diagram of droplet detachment sensor system components.

Detachment time intervals were measured for a number of electrode speeds using the variation in the acquired electrode-to-workpiece voltage. A typical voltage signal, after filtering to remove the low-frequency variations, showed a series of bipolar spikes. Each bipolar spike in the signal corresponded to a droplet detachment. A computer program was written to detect these detachments using the voltage signal and to calculate the average and range of detachment time intervals.

High-Speed Movies

High-speed movies were made using a laser back-lighting technique [23] to suppress the arc light and produce a silhouette of the electrode and droplets. A semiautomatic image analysis system was developed to obtain information about the droplets, including time between detachments, electrode position, droplet volume, and droplet kinematics. A frame of the film was projected on a film viewer and the image was transferred to a computer using a video camera and a frame grabber. The image was then enhanced to produce outlines of the electrode and the droplets. From these outlines the projected area and position of each droplet as a function of time were determined. The detachment time for each droplet could also be determined using timing marks placed in the region of the film between the sprocket marks. These timing marks were also recorded synchronously with the electrical data so that a one-to-one correspondence between that data and the film could be made. Figure 6 shows a typical frame, taken just after droplet detachment.

The volume of the droplets was calculated by measuring the area of the silhouette in square pixels for 10 to 20 frames after detachment. The average of these measurements was assumed to be the projected area of the equivalent sphere and the volume was calculated using this assumption. This averaging procedure also smoothes some of the quantum effects due to the finite pixel size. The droplet silhouettes are actually observed to oscillate from a distorted, elongated shape (see Fig. 6), to a circular shape, and then to a slightly flattened circular shape. Some larger droplets also showed flattened sides as they oscillated about the assumed equilibrium spherical shape.

Electrical Signals

The detachment time intervals are summarized in Table 2. The structure of the data can be seen better in Figure 7, where the percentage of droplets falling in a particular detachment time range is plotted as a function of the detachment time and the electrode speed. The range of detachment times (0.1 ms to 1 s) is divided logarithmically into 50 bins. A gray scale ranging from white, corresponding to less than 1%, to black, corresponding to greater than 28%, is used to show detachments.

The data at the upper left of Figure 7 is from pure globular transfer with droplet diameters greater than the electrode diameter. As the electrode speed increases, a transition to shorter detachment times and smaller droplets is observed; at about 140 mm/s the system appears to transition to spray transfer. This can be seen from the second set of droplets with a much shorter detachment time that appears in the lower right-hand portion of Figure 7. This second set of droplets, however, then merges with the original set where most of the droplets are again larger than the electrode diameter, corresponding to globular transfer. Thus, these data indicate that no sharp transition between globular transfer and spray transfer exists. Rather, small droplets gradually become more prominent and the percentage of

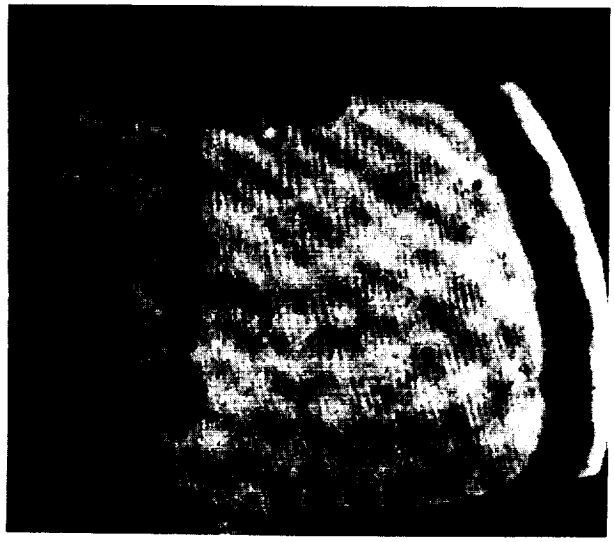

Figure 6. Back-lighted image of a globular droplet just after detachment.

Table 2. Summary of Detachment Times

Electrode Speed (mm/s)	DC Current (A)	Ave. Time (ms)	Range of Times (ms)	Electrode Speed (mm/s)	DC Current (A)	Ave. Time (ms)	Range of Times (ms)
55	90	379	114-689	115	163	52	9.9-142
60	94	311	59-543	120	167	48	13-140
65	97	251	37-435	125	176	36	6.8-62
70	106	218	37-560	130	184	28	2.3-59
75	112	196	62-418	135	180	21	1.9-126
80	124	160	20-265	140	184	18	0.8-77
85	135	136	26-285	145	187	12	0.2-48
90	139	106	15-208	150	195	8.1	0.1-27
95	142	89	32-196	155	195	10.3	1.7-21
100	148	77	26-214	160	197	5.0	0.2-30.5
105	150	65	9.9-140	165	190	8.2	2.2-15.1
110	154	57	2.3-160	170	190	6.8	0.5-13.8

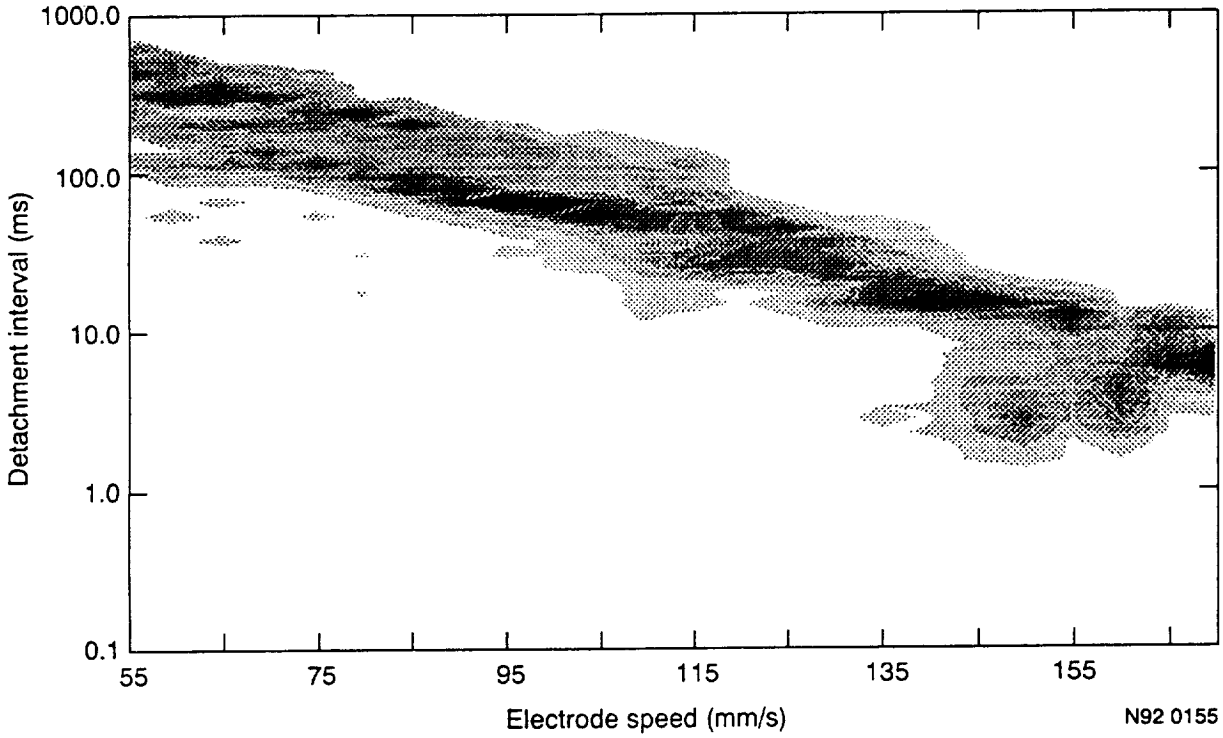

Figure 7. Distribution of droplet detachment interval as a function of electrode speed from experimental data.

larger droplets decreases as the electrode speed and current increase through the transition region. However, more data are required to characterize the transition fully. A model of this process, discussed briefly in the next section, shows a similar trend [30].

High-speed Film Analysis

If the electrode melted at a constant rate, independent of droplet size, the measured time interval between detachments versus the volume of the droplet would lie on a straight line, whose slope could be calculated from

the electrode speed and the electrode size. The data do not follow such lines. The smaller droplets are generally below the line, while a few larger droplets are above the line. This implies that the smaller droplets are detaching in less time than the average, that the electrode is getting shorter, and that the arc length is increasing as each small droplet detaches. The arc length, therefore, may have a very important role in determining melting rate and droplet size.

It was also observed that a particularly large droplet was often followed by a series of small droplets. During the detachment of the large droplet, the electrode extension increased, since these droplets melted slower than average. After a series of small droplet detachments, the electrode extension decreased, since these melted faster than average. This cycle sometimes repeated itself several times, with one or two large droplets followed by a series of small droplets, followed by another one or two large droplets, etc.

The kinematics of the falling droplets was also measured by determining the position of the center of the droplet as a function of time. These position data were then fit to a linear and to a quadratic function. For electrode speeds of 130 and 140 mm/s, the acceleration of the droplet determined in the quadratic fit was negligible and the data was fit just as well by a straight line. Thus the net force on the drop must be zero.

A plot of the reciprocal of the droplet velocity versus the area of the droplet was approximately a straight line, as would be expected from a Stoke's law friction force on the droplet. However, the data showed significant scatter, possibly corresponding to the fact that the droplet shape oscillates and is not spherical.

Discussion of Experimental Results

According to the standard definitions of globular and spray transfer, the distinguishing characteristic is the size of the droplet relative to the electrode size. However, in these experiments the experienced welding technician perceived that the process was in spray mode for electrode speeds above about 160 mm/s. This expert opinion was based on the sound of the process and the observation of a taper on the electrode [22]. Perhaps the standard definition is not exact enough for these purposes. The detachment time data for these experiments indicate that a large fraction of the droplets were larger than the electrode diameter. A more practical definition may be related to the fact that the penetration is greater in spray transfer. The penetration depends on the droplet momentum when it enters the pool [31], which depends not only on the droplet size, as shown here, but on the continued acceleration of the droplet after detachment. Very large accelerations (10 G) have been observed in spray transfer [19].

Further experiments are planned using both high-speed film and electrical sensing. Other parameters will be varied, including contact-tip-to-workpiece distance and open-circuit voltage. Observation of the spray region is limited since the bipolar voltage signal associated with the detachment decreases as the droplet size decreases and approaches the noise level. This makes it difficult to measure the detachment times at higher currents using electrical sensing.

Theoretical Investigation

The physics of droplet transfer in GMAW is analogous to water dripping or flowing from an orifice [26]. Shaw [32] showed that a dripping faucet is an example of a system of chaotic transitions, i.e., the system can change from a periodic and predictable to an aperiodic, quasi-random pattern of behavior as a single parameter (in this case, flow rate) is varied. The purpose of this work is to develop a dynamic droplet growth and detachment model that predicts droplet size and transfer frequencies in the globular and spray transfer modes, as well as in the transition region between the two modes, by extending the Shaw model.

Droplet Growth and Detachment Theories

A major theory on the growth and detachment of GMAW droplets is the static force balance theory. Kim and Eagar [33] showed that this theory gives good correlation between experimental and predicted values for droplet size in the globular transfer mode but deviates significantly in the spray transfer mode. The static force

REFERENCES

1. Lott, L. A.; Johnson, J. A.; and Smartt, H. B. 1983. Proceedings, 1983 Symposium on Nondestructive Evaluation Applications and Materials Processing, 13-22.

2. Johnson, J. A.; and Carlson, N. M. 1986. NDT International, 19: 190-196.

3. Carlson, N. M.; and Johnson, J. A. 1986. Review of Progress in Quantitative Nondestructive Evaluation 5A: 773-780.

4. Carlson, N. M.; Johnson, J. A.; and Kunerth, D. C. 1990. Welding Journal 69: 256s-263s.

5. Johnson, J. A.; and Carlson, N. M. 1990. Review of Progress in Quantitative Nondestructive Evaluation 10: 2097-2104.

6. Johnson, J. A. 1988. Review of Progress in Quantitative Nondestructive Evaluation 7: 1485-1494.

7. Carlson, N. M.; and Johnson, J. A. 1988. Review of Progress in Quantitative Nondestructive Evaluation 7: 1485-1494.

8. Clark, A. V.; Fortunko, C. M.; Schaps, S. R.; and Capobianco, T. E. Proceedings, IEEE Symposium on Ultrasonics, Ferroelectronics, and Frequency Control, Orlando, FL, 1991, to be published.

9. Agapakis, J. E.; Katz, J. M.; Koifman, M.; Epstein, G. N.; Friedman, J.M.; Eyring, D. O.; and Rutishauser, H. J. 1986. Welding Journal 65(11): 33-41.

10. Hanright, J. 1986. Welding Journal 65(11): 19-24.

11. Richardson, R. W.; Gutow, D. A.; Anderson, R. A.; and Farson, D.F. 1984. Welding Journal 63(3): 43-50.

12. Lukens, W. E.; and Morris, R. A. 1982. Welding Journal 61(1): 27-33.

13. Duncan, R. 1990. Extending DOS: Reading, Massachusetts: Addison-Wesley Publishing Company.

14. Phar Lap Software. 1989. 386|DOS-Extender.

15. Pratt, W. K. 1978. Digital Image Processing: New York: Wiley.

16. Gonzalez, R. C.; and Wintz, P. 1977. Digital Image Processing: Reading, Massachusetts: Addison-Wesley.

17. Kreith, F.; and Bohn, M. S. 1986. Principles of Heat Transfer: p. 429, New York: Harper and Row Publishers.

18. Watkins, A. D. 1989. Heat transfer efficiency in gas metal arc welding. M.S. Thesis, University of Idaho.

19. Clark, D. E.; Buhrmaster, C. L.; Smartt, H. B. 1989. Drop transfer mechanism in GMAW. Proc. Trends in Welding Research, eds. by S. David and J. Vitak, Gatlinburg, TN.

20. Lesnewich, A. 1958. Control of melting rate and metal transfer in gas-shielded metal arc welding, part II - control of metal transfer. Welding Journal 37(9): 418s-425s.

21. Adam , G.; and Siewert, T. A. 1990 Sensing of GMAW droplet transfer modes using an ER100S-1 electrode. Welding Journal 69(3): 103s-108s.

22. Kim, Y.-S.; McEligot, D. M. and Eagar, T. W. , 1991. Welding Journal 70(1): 20s-31s.

23. Allemand, C. D.; Schoeder, R.; Ries, D. E.; Eagar, T. W. 1985. Welding Journal 64: 45-47.

24. Amson, J. C. 1962. An analysis of the gas-shielded consumable metal arc welding system," British Welding Journal 41(4): 232-249.

25. Waszink, J. H.; and Graat, L. H. J. 1983. Experimental investigation of the forces acting on a drop of weld metal. Welding Journal 62(4): 109s-116s.

26. Lancaster, J. F. 1984. The Physics of Welding: Oxford: Pergamon Press.

27. Allum, C. J. 1985. Metal transfer in arc welding as a varicose instability: I. varicose instability in a current-carrying liquid cylinder with surface charge. *and* II. development of a model for arc welding. Journal of Physics D: Applied Physics 18: 1431-1468.

28. Johnson, J. A.; Carlson, N. M.; Smartt, H. B.; and Clark, D. E. 1991. Welding Journal 70: 91s-99s.

29. Johnson, J. A.; Smartt, H. B.; Clark, D. E.; Carlson, N. M.; Watkins, A. D.; Lethcoe, B. J. 1990. Proc. Conf. on Modeling of Casting, Welding and Solidification Processes, Engineering Foundation, Davos, Switzerland.

30. Watkins, A. D.; Smartt, H. B.; Johnson, J. A. 1992. 3rd International Conference on Trends in Welding Research, Gatlinburg, Tennessee.

31. Essers W. G.; and Walter, R. 1981. Welding Journal 60: 37s-42s.

32. Shaw, R. 1984. The Dripping Faucet as a Model Chaotic System The Science Frontier Express, Aerial Press, Inc.

33. Eagar, T. W. 1992. Personal communication, Massachusetts Institute of Technology, Cambridge, MA.